Optics Letters

Design of broadband and wide-field-of-view metalenses

Fan Yang,[1,5] Sensong An,[2] Mikhail Y. Shalaginov,[1] Hualiang Zhang,[2] Clara Rivero-Baleine,[3] Juejun Hu,[1,4] and Tian Gu[1,4,*]

[1]Department of Materials Science & Engineering, Massachusetts Institute of Technology, Cambridge, Massachusetts 02139, USA
[2]Department of Electrical & Computer Engineering, University of Massachusetts Lowell, Lowell, Massachusetts 01854, USA
[3]Lockheed Martin Corporation, Orlando, Florida 32819, USA
[4]Materials Research Laboratory, Massachusetts Institute of Technology, Cambridge, Massachusetts 02139, USA
[5]e-mail: yangf@mit.edu
*Corresponding author: gutian@mit.edu

Received 3 August 2021; revised 13 October 2021; accepted 26 October 2021; posted 28 October 2021; published 15 November 2021

In this Letter, we adapt the direct search method to metasurface optimization. We show that the direct search algorithm, when coupled with deep learning techniques for free-form meta-atom generation, offers a computationally efficient optimization approach for metasurface optics. As an example, we apply the approach to optimization of achromatic metalenses. Taking advantage of the diverse dispersion responses of free-form meta-atoms, metalenses designed using this approach exhibit superior broadband performances compared to their multilevel diffractive counterparts. We further demonstrate an achromatic and wide-field-of-view metalens design.

https://doi.org/10.1364/OL.439393

Optical metasurfaces (also known as sub-wavelength diffractive optics), which leverage sub-wavelength structures to sculpt the wavefront of light, have been widely recognized as a promising technology potentially enabling optical systems with significant size, weight, and performance advantages [1–5]. Broadband operation, however, has been a standing challenge for metasurface optics [6]. A number of techniques have been implemented to realize achromatic metalenses. One solution involves dispersion engineering of individual meta-atoms to compensate for chromatic aberration [7–14]. The objective of this approach is to assemble a metalens out of meta-atoms with target dispersion behaviors such that hyperbolic phase profiles corresponding to the same focal length are fulfilled at different wavelengths. Another scheme termed "zone engineering" has been demonstrated recently [15], where the locations and step sizes for phase wrap are judiciously engineered to maximize the phase coherence at the focal spot. Full-aperture optimization methods (instead of relying on discrete meta-atoms) [16–19] and cascaded metasurface designs [20] have also been developed, although the computational load becomes prohibitively large when these methods are applied to large-aperture (mm to cm scale) optics. Finally, computational imaging has been proven to be a powerful technique to retrieve high-quality broadband images when coupled with front-end meta-optics engineering [21,22].

Direct search (DS) optimization is an alternative technique that has been explored for broadband optics design [23–27]. In the seminal work by Menon *et al.*, it has been shown that by constraining only the intensity while leaving optical phase as a free parameter, broadband achromatic flat lenses can be realized with enhanced performance given the extra degrees of freedom in phase selection [28]. In their studies, the DS algorithm was implemented to optimize only multilevel diffractive optics, where the individual unit cells or pixels consist of a film with varying thicknesses. The phase delay imparted by the unit cells therefore invariably follows a $1/\lambda$ dependence.

In this Letter, we adapt the DS algorithm to optimization of metalenses comprising free-form meta-atoms. By combining the DS algorithm with a deep neural network trained for free-form meta-atom generation, we demonstrate that the diverse dispersion behaviors of the free-form meta-atoms lead to superior performance of the metalenses compared to their diffractive counterparts optimized using the same algorithm and parameter sets. To illustrate that the approach is generically applicable to different metalens configurations, we further implement the technique to design an achromatic fisheye metalens with 200 nm spectral bandwidth in the near-IR.

Our design process starts with generation of a set of meta-atoms with diverse dispersion responses. The generation process capitalizes on our recently developed deep learning algorithm targeting metasurfaces with high degrees of freedom [29,30], which rapidly yields broadband optical responses (amplitude and phase) of free-form meta-atoms without resorting to full-wave electromagnetic simulations [31,32]. We started with 3000 randomly generated meta-atom structures using a needle-drop method [29]. Figure S1 in Supplement 1 depicts the top-view layouts of several randomly selected examples of the meta-atoms. All meta-atoms in the library are patterned from a 1.4 μm thick Si layer resting on a SiO_2 substrate with a uniform period (pitch) of 0.5 μm. The amplitude and phase responses of the meta-atoms modeled using the deep neural network and full-wave simulations are also compared in Fig. S1,

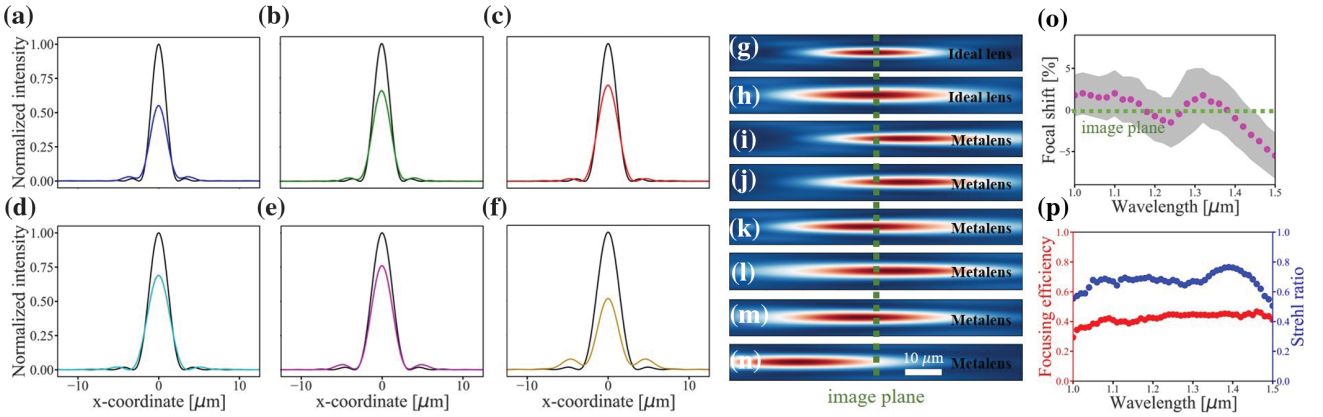

Fig. 1. (a)–(f) Normalized intensity distributions of the focal spot on image plane at wavelengths of (a)1.0 μm, (b)1.1 μm, (c)1.2 μm, (d)1.3 μm, (e)1.4 μm, and (f)1.5 μm from the broadband metalens (color lines) and an ideal aberration-free lens (black lines). (g), (h) Normalized intensity distribution along the optical axis for an aberration-free lens at wavelengths of (g) 1.0 μm and (h) 1.5 μm. (i)–(n) Normalized intensity distribution along the optical axis for the broadband metalens at wavelengths of (i) 1.0 μm, (j) 1.1 μm, (k) 1.2 μm, (l) 1.3 μm, (m) 1.4 μm, and (n) 1.5 μm. (o) Longitudinal chromatic focal shift of the metalens: the shaded area represents focal tolerance (defined as the longitudinal range where the on-axis intensity is above 80% of the peak intensity at the focal spot). (p) Focusing efficiency and Strehl ratio of the metalens.

showing excellent agreement between the two approaches. In this study, we did not target any specific pre-defined meta-atom dispersion when compiling the meta-atom library.

The 3000 meta-atoms form the library for subsequent DS optimization. We verified that further expanding the library brings marginal benefits, implying that the library already covers the entire accessible meta-atom design space given the geometric conditions (see Supplement 1). The flow chart of the DS algorithm is shown in Fig. S2. The Kirchhoff diffraction integral was used to evaluate the focusing performance of the lens.

This combination of DS optimization and a deep learning algorithm is ideally suited for versatile and computationally efficient metasurface design. The deep learning algorithm is capable of rapidly generating a large number of meta-atom designs, whose free-form layouts enable the exploration of many geometric degrees of freedom to enable a wide range of dispersion properties and thereby maximally boost performance. DS also copes well with the large varieties of meta-atoms, which otherwise can present a throughput challenge for alternative optimization schemes. This is because the DS optimization is sequentially and locally performed on each meta-atom. During the performance evaluation step, partial diffraction integrals representing the contribution from all meta-atoms other than the one being replaced remain constant and thus do not need to be re-computed. Moreover, the diffraction integral evaluation is an "embarrassingly parallel" task and was thus executed leveraging a commercial cloud computing service to drastically reduce the iteration time. For this reason, the approach can be readily scaled to metasurfaces with large (cm scale) optical apertures.

The main assumption of the optimization scheme is that mutual coupling between meta-atoms is insignificant. This assumption is a reasonable approximation for high-index meta-atoms with strong field confinement. However, corrections must be applied when such coupling is not negligible [33].

Our first design example is an achromatic single-layer metalens operating across the 1–1.5 μm spectral range with a diameter of 200 μm and focal length (f) of 400 μm, corresponding to a numerical aperture (NA) of 0.24. Cross-sectional intensity distributions of the focal spot at several wavelengths and on the same image plane ($f = 400$ μm) are displayed in Figs. 1(a)–1(f), alongside the focal spot profiles from an ideal aberration-free lens of the same NA. Intensity distributions along the optical axis at these wavelengths are displayed in Figs. 1(i)–1(n), alongside the intensity distributions from an ideal aberration-free lens at wavelengths of 1.0 μm and 1.5 μm shown in Figs. 1(g)–1(h). The average longitudinal chromatic focal shift is 1.6% over the spectral range [Fig. 1(o)]. The relatively small chromatic focal shift ensures that the fixed image plane falls within focal tolerance of the lens throughout most of the spectral band, which accounts for the high Strehl ratio. The wavelength-dependent focusing efficiency (defined as the fraction of power encircled within an area of a diameter equaling three times the focal spot full-width-at-half-maximum normalized by the total incident power) and Strehl ratio calculated using the Kirchhoff diffraction integral are plotted in Fig. 1(p). The design yields a spectrally averaged focusing efficiency of 42% and Strehl ratio of 0.67.

As a comparison, we applied the same optimization approach to multilevel diffractive lenses (MDLs). In MDLs, the height of unit cells on the lens surface is utilized to control the phase response of the broadband lens. In the optimization, the same unit cell period of 0.5 μm and maximum layer thickness of 1.4 μm are assumed for both metalenses and MDLs. It is important to note that the broadband performances of both

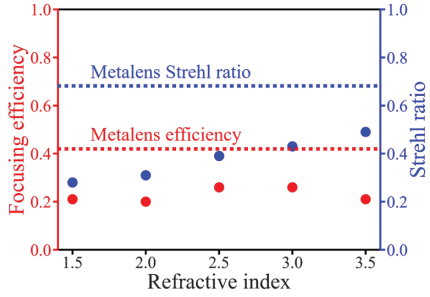

Fig. 2. 1–1.5 μm wavelength-averaged focusing efficiency and Strehl ratio of MDLs with varying diffractive surface refractive indices. The dashed lines give performances of the metalens shown in Fig. 1.

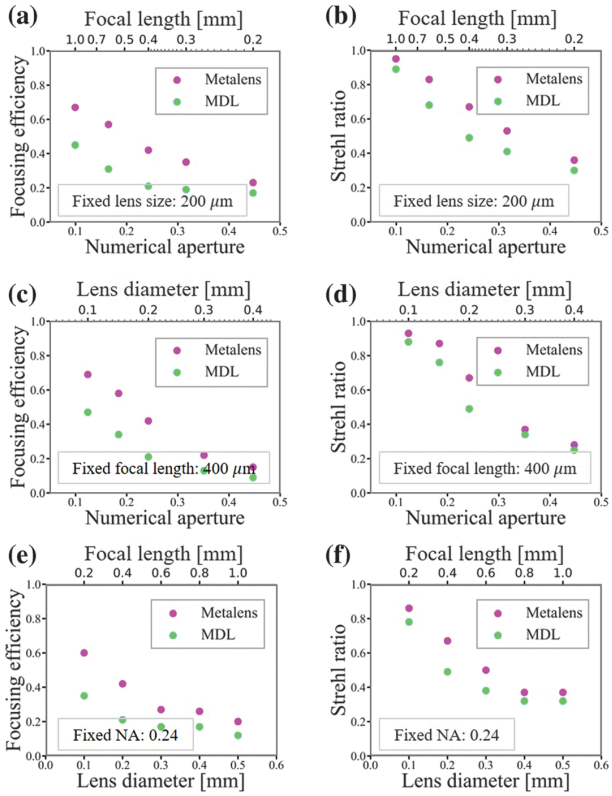

Fig. 3. Performance comparison between metalens and MDLs with varying design parameters, showing spectrally averaged focusing efficiency and Strehl ratio as functions of: (a), (b) NA with varying focal lengths; (c), (d) NA with varying lens aperture sizes; and (e), (f) aperture size with constant NA.

metalenses and MDLs improve with increasing unit cell height, since the group delay increases with larger thickness [6,34]. Therefore, the same thickness is assumed for the sake of drawing a fair comparison. Figure 2 compares the simulated wavelength-averaged focusing efficiency and Strehl ratio of the metalens in Fig. 1 and MDLs with diffractive surface refractive indices varying from 1.5 to 3.5. The metalens offers superior efficiency and Strehl ratio compared to the MDLs due to the diverse dispersion characteristics of the free-form meta-atoms.

We further extend the comparison of flat lenses considering a wide range of design parameters. Figure 3 compares the spectrally averaged focusing efficiency and Strehl ratio of metalenses and MDLs of varying NAs and aperture sizes, both optimized using the DS approach over the 1–1.5 μm band. The diffractive surface refractive index of MDLs is set to 3.5 with a maximum thickness of 1.4 μm, the same as the metalens design. The performances of metalenses based on free-form meta-atoms are consistently superior to or at least on par with their MDL counterparts. The result highlights facile dispersion engineering as an important advantage of free-from meta-atom structures [35,36], where their increased geometric degrees of freedom enable tailoring of waveguiding and multipole resonance behaviors to produce favorable dispersion responses [37,38].

Finally, we demonstrate that the DS + deep learning design paradigm can also be harnessed to realize advanced metalens architectures. As an example, here for the first time, we present the design of a wide-field-of-view (FOV) and broadband achromatic metalens. The configuration of the lens is illustrated in Fig. S3 in Supplement 1. The phase profile of the backside metasurface is optimized using the DS algorithm with the angle of incidence (AOI)-dependent image height (lateral displacement of the focal spot with respect to the optical axis) given by a closed-form expression [39]:

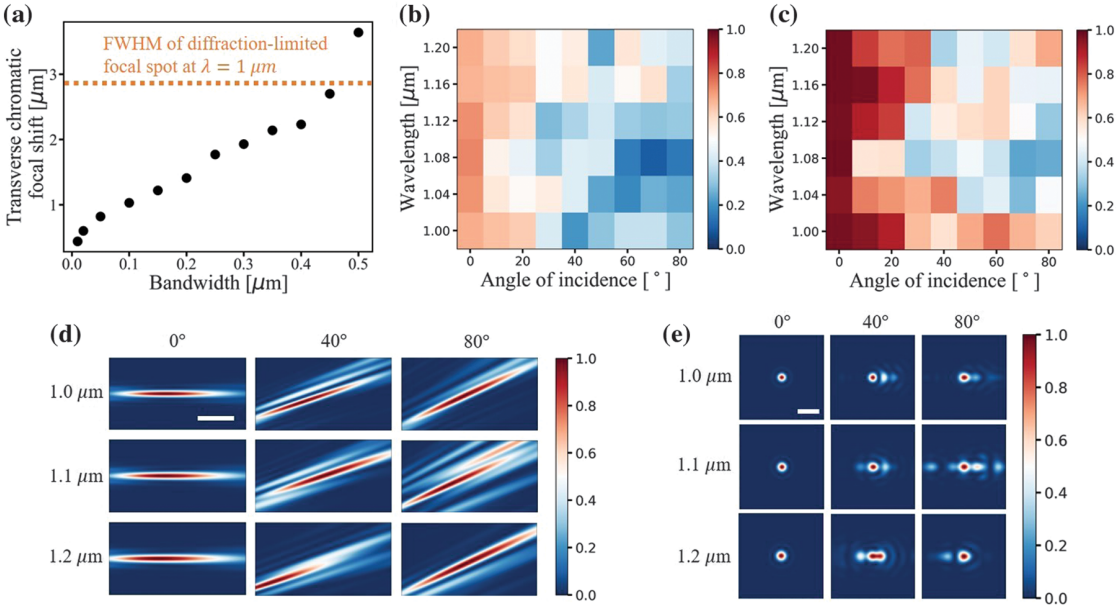

Fig. 4. Broadband and wide-FOV metalens performance characterization. (a) Transverse chromatic focal shift (averaged over the full 180° FOV and the 1–1.2 μm spectral range) relative to the analytically derived image heights in Eq. (1) for wide-FOV metalenses with varying bandwidths. Here the lower end of the wavelength is fixed at 1 μm. (b) Focusing efficiency and (c) Strehl ratio dependences on both wavelength and AOI. (d) Axial intensity distributions of the focal spot on the meridional plane at different wavelengths and AOIs (scale bar: 20 μm). Centers of all the figures are the focal spot position derived from Eq. (1) on the image plane. (e) Intensity distributions on the image plane at different wavelengths and AOIs (scale bar: 10 μm).

$$\Delta d = \left[\left(\frac{L\sin\alpha}{\sqrt{n^2-\sin^2\alpha}} - d\right)^2 + f^2\right]^{\frac{3}{2}} \left(\frac{\cos\alpha}{f^2}\right)\Delta\alpha. \quad (1)$$

In the equation, d is the image height, $n = 1.45$ denotes the substrate refractive index, α represents the AOI, $L = 200$ μm is the substrate thickness, and the focal length is set to $f = 280$ μm. The top aperture has a diameter of 100 μm. This equation is exact for a single-wavelength design. As bandwidth increases, transverse chromatic aberration becomes more pronounced, and the in-plane focal spot position progressively deviates from the equation (see Supplement 1). We note that this effect is unique to wide-FOV lenses; prior achromatic metalens designs were constrained to a small on-axis FOV, and the transverse chromatic aberration is insignificant. Figure 4(a) presents the AOI and wavelength averaged transverse chromatic focal shift as a function of metalens spectral bandwidth. The wide-FOV metalens bandwidth becomes limited by the transverse chromatic aberration rather than the axial chromatic focal shift.

We choose an exemplary design operating across the 1–1.2 μm wavelength range and targeting 180° FOV, using the same meta-atom library as in the preceding examples. Within the spectral range, the transverse chromatic focal shift is far smaller than the focal spot size, and thus the lens is close to achromatic. The results are shown in Figs. 4(b)–4(e). The Kirchhoff diffraction integral was applied to calculate the focusing efficiency and Strehl ratio of the broadband and wide-FOV metalens. It maintains high focal spot quality across the entire 1–1.2 μm band and FOV with an average focusing efficiency of 45% and a Strehl ratio of 0.64.

In summary, we demonstrate that the combination of DS optimization and deep learning meta-atom generation networks presents a generic and computationally efficient scheme for objective-driven design of metasurface optics. We show that meta-optics designed using the scheme offer enhanced performances over their MDL counterparts, exploiting the diverse dispersion characteristics of the free-form meta-atoms that form the metasurface. We further applied the scheme to develop the first broadband and wide-FOV metalens design.

Funding. MIT Skoltech Seed Fund Program; DARPA EXTREME Optics and Imaging Program (HR00111720029); Lockheed Martin Corporation Internal Research and Development.

Acknowledgment. The authors gratefully acknowledge helpful discussions with Jeremy Teichman at the Institute for Defense Analyses.

Disclosures. The authors declare no conflicts of interest.

Data Availability. All simulation data that support the findings of this study are available upon reasonable request.

Supplemental document. See Supplement 1 for supporting content.

REFERENCES

1. N. Yu, P. Genevet, M. A. Kats, F. Aieta, J.-P. Tetienne, F. Capasso, and Z. Gaburro, Science **334**, 333 (2011).
2. A. V. Kildishev, A. Boltasseva, and V. M. Shalaev, Science **339**, 1232009 (2013).
3. P. Lalanne and P. Chavel, Laser Photon. Rev. **11**, 1600295 (2017).
4. S. B. Glybovski, S. A. Tretyakov, P. A. Belov, Y. S. Kivshar, and C. R. Simovski, Phys. Rep. **634**, 1 (2016).
5. S. M. Kamali, E. Arbabi, A. Arbabi, and A. Faraon, Nanophotonics **7**, 1041 (2018).
6. F. Presutti and F. Monticone, Optica **7**, 624 (2020).
7. S. Wang, P. C. Wu, V.-C. Su, Y.-C. Lai, M.-K. Chen, H. Y. Kuo, B. H. Chen, Y. H. Chen, T.-T. Huang, J.-H. Wang, R.-M. Lin, C.-H. Kuan, T. Li, Z. Wang, S. Zhu, and D. P. Tsai, Nat. Nanotechnol. **13**, 227 (2018).
8. W. T. Chen, A. Y. Zhu, V. Sanjeev, M. Khorasaninejad, Z. Shi, E. Lee, and F. Capasso, Nat. Nanotechnol. **13**, 220 (2018).
9. S. Shrestha, A. C. Overvig, M. Lu, A. Stein, and N. Yu, Light Sci. Appl. **7**, 85 (2018).
10. M. Khorasaninejad, Z. Shi, A. Y. Zhu, W.-T. Chen, V. Sanjeev, A. Zaidi, and F. Capasso, Nano Lett. **17**, 1819 (2017).
11. E. Arbabi, A. Arbabi, S. M. Kamali, Y. Horie, and A. Faraon, Optica **4**, 625 (2017).
12. Q. Cheng, M. Ma, D. Yu, Z. Shen, J. Xie, J. Wang, N. Xu, H. Guo, W. Hu, S. Wang, T. Li, and S. Zhuang, Sci. Bull. **64**, 1525 (2019).
13. S. Wang, P. C. Wu, V.-C. Su, Y.-C. Lai, C. H. Chu, J.-W. Chen, S.-H. Lu, J. Chen, B. Xu, C.-H. Kuan, T. Li, S. Zhu, and D. P. Tsai, Nat. Commun. **8**, 187 (2017).
14. A. Ndao, L. Hsu, J. Ha, J.-H. Park, C. Chang-Hasnain, and B. Kanté, Nat. Commun. **11**, 3205 (2020).
15. Z. Li, P. Lin, Y.-W. Huang, J.-S. Park, W. T. Chen, Z. Shi, C.-W. Qiu, J.-X. Cheng, and F. Capasso, Sci. Adv. **7**, eabe4458 (2021).
16. D. Sell, J. Yang, S. Doshay, R. Yang, and J. A. Fan, Nano Lett. **17**, 3752 (2017).
17. H. Chung and O. D. Miller, Opt. Express **28**, 6945 (2020).
18. Z. Lin, C. Roques-Carmes, R. E. Christiansen, M. Soljačić, and S. G. Johnson, Appl. Phys. Lett. **118**, 041104 (2021).
19. R. E. Christiansen, Z. Lin, C. Roques-Carmes, Y. Salamin, S. E. Kooi, J. D. Joannopoulos, M. Soljačić, and S. G. Johnson, Opt. Express **28**, 33854 (2020).
20. Z. Huang, M. Qin, X. Guo, C. Yang, and S. Li, Opt. Express **29**, 13542 (2021).
21. Z. Lin, C. Roques-Carmes, R. Pestourie, M. Soljačić, A. Majumdar, and S. G. Johnson, Nanophotonics **10**, 1177 (2020).
22. E. Tseng, S. Colburn, J. Whitehead, L. Huang, S.-H. Baek, A. Majumdar, and F. Heide, "Neural nano-optics for high-quality thin lens imaging," arXiv:2102.11579 (2021).
23. P. Wang, N. Mohammad, and R. Menon, Sci. Rep. **6**, 21545 (2016).
24. P. Wang, J. A. Dominguez-Caballero, D. J. Friedman, and R. Menon, Prog. Photovoltaics **23**, 1073 (2015).
25. P. Wang and R. Menon, J. Micro/Nanolithography, MEMS, MOEMS **14**, 023507 (2015).
26. P. Wang and R. Menon, Opt. Express **22**, 14575 (2014).
27. P. Wang and R. Menon, Opt. Express **21**, 6274 (2013).
28. M. Meem, S. Banerji, A. Majumder, J. C. Garcia, P. W. Hon, B. Sensale-Rodriguez, and R. Menon, "Imaging from the visible to the longwave infrared wavelengths via an inverse-designed flat lens," arXiv:2001.03684 (2020).
29. S. An, B. Zheng, M. Y. Shalaginov, H. Tang, H. Li, L. Zhou, J. Ding, A. M. Agarwal, C. Rivero-Baleine, M. Kang, K. A. Richardson, T. Gu, J. Hu, C. Fowler, and H. Zhang, Opt. Express **28**, 31932 (2020).
30. S. An, C. Fowler, B. Zheng, M. Y. Shalaginov, H. Tang, H. Li, L. Zhou, J. Ding, A. M. Agarwal, C. Rivero-Baleine, K. A. Richardson, T. Gu, J. Hu, and H. Zhang, ACS Photon. **6**, 3196 (2019).
31. P. R. Wiecha and O. L. Muskens, Nano Lett. **20**, 329 (2019).
32. M. V. Zhelyeznyakov, S. Brunton, and A. Majumdar, ACS Photon. **8**, 481 (2021).
33. S. An, B. Zheng, M. Y. Shalaginov, H. Tang, H. Li, L. Zhou, Y. Dong, M. Haerinia, A. M. Agarwal, C. Rivero-Baleine, M. Kang, K. A. Richardson, T. Gu, J. Hu, C. Fowler, and H. Zhang, "Deep convolutional neural networks to predict mutual coupling effects in metasurfaces," arXiv:2102.01761 (2021).
34. J. Engelberg and U. Levy, Optica **8**, 834 (2021).
35. S. Banerji, M. Meem, A. Majumder, F. G. Vasquez, B. Sensale-Rodriguez, and R. Menon, Optica **6**, 805 (2019).
36. J. Engelberg and U. Levy, Nat. Commun. **11**, 1991 (2020).
37. S. An, B. Zheng, H. Tang, M. Y. Shalaginov, L. Zhou, H. Li, M. Kang, K. A. Richardson, T. Gu, J. Hu, C. Fowler, and H. Zhang, Adv. Opt. Mater. **9**, 2001433 (2021).
38. M. Y. Shalaginov, S. D. Campbell, S. An, Y. Zhang, C. Ros, E. B. Whiting, Y. Wu, L. Kang, B. Zheng, C. Fowler, H. Zhang, D. H. Werner, J. Hu, and T. Gu, Nanophotonics **9**, 3505 (2020).
39. F. Yang, S. An, M. Y. Shalaginov, H. Zhang, J. Hu, and T. Gu, "Wide field-of-view flat lens: an analytical formalism," arXiv:2108.09295 (2021).